

# Hydrogen Radical Detection in Catalytic Hydrogenation Reactions: Background C-H Activation in Solvents

Hannah Rogers,<sup>[a]</sup> Timothy J. Woodman,<sup>[b]</sup> David J. Willock,<sup>[c]</sup> Andrea Folli,<sup>[c]</sup> and Simon J. Freakley\*<sup>[a]</sup>

Platinum group metal (PGM) nanoparticle catalysts are commonly used in a wide variety of liquid-phase hydrogenation reactions. Carbon-supported palladium nanoparticles are used extensively in many industrially applied hydrogenation reactions across the pharmaceutical industry and increasingly in the hydrogenolysis of bio-derived molecules. These reactions are often performed in solvents such as toluene or xylene which are considered inert towards mild hydrogenation condi-

tions. Through a series of catalytic studies analysed using <sup>1</sup>H/<sup>2</sup>H Nuclear Magnetic Resonance (NMR) and Electron Paramagnetic Resonance (EPR) spectroscopies, and Density Functional Theory (DFT) calculations, we present evidence that hydrogen is being constantly exchanged into the methyl groups of the solvent possibly via a radical mechanism at these mild conditions. These effects should be considered in the explanation of any model of catalytic hydrogenation reaction at metal surfaces.

## 1. Introduction

Hydrogenation reactions using heterogeneous catalysts are widely studied in industry and academia with applications in the production of pharmaceuticals, agrochemicals, fine chemicals, and hydrotreatments of petrochemical and bio-derived feedstocks.<sup>[1]</sup> As such, hydrogenation reactions account for 10%–20% of all industrial chemical steps and will remain an essential catalytic technology to add value to renewable resources.<sup>[2]</sup> Catalysts containing metallic palladium (Pd) nanoparticles (typically 1–50 nm) and bimetallic particles containing Pd have been developed for a wide range of hydrogenative transformations including complete or selective hydrogenations of alkenes, alkynes, carbonyls, and nitro compounds in addition to hydrogenolysis of C–O/C–C bonds in biomass or polymer upgrading.<sup>[3]</sup> The prevalence of Pd as a hydrogenation catalyst is clear in both the academic and patent literature due to H<sub>2</sub> dissociation on Pd proceeding with a low energy barrier.<sup>[4]</sup>

Our understanding of hydrogenation on Pd surfaces developed from the mechanism proposed for alkene hydrogenation in 1934. The so-called Horiuti–Polanyi mechanism is described as a series of reaction steps leading to saturation of the alkene double bond: i) H<sub>2</sub> dissociation at the catalyst surface to form atomic surface hydrogen, H\*, ii) formation of a π-complex between the alkene and Pd surface, iii) sequential addition of H\* to the substrate, iv) saturated product desorption – this mechanism is almost universally recognized as the basis for many reactions on metal surfaces with low barriers to H<sub>2</sub> dissociation in both the gas and liquid phase.<sup>[5]</sup> More recently evidence of an additional redox mechanism has been reported for the hydrogenation of O<sub>2</sub> to form H<sub>2</sub>O<sub>2</sub> and the hydrogenation of furanic compounds in protic media which draws an analogy to enzymatic hydrogenases or electrochemical reactions.<sup>[6–8]</sup> These proposed mechanisms concern proton-coupled-electron-transfer (PCET) of hydrogen oxidation (H<sub>2</sub> ⇌ 2H<sup>+</sup> + 2e<sup>−</sup>) and C = C/O reduction via water-mediated proton transfer participating directly in the kinetically relevant reaction step.

An overlooked consideration in the description of surface hydrogenation processes is the presence and reactivity of weakly bound atomic H ad-atoms (H<sub>(w)</sub>\*) with free radical-like character in contrast to the strongly bound surface species. The study of free radicals in hydrogenation chemistry was initiated by Howe and co-workers in 1980 using spin trap experiments to demonstrate the radical character of certain adsorption modes of H<sub>2</sub> on ZnO catalysts used for gas phase alkene hydrogenation.<sup>[9]</sup> Through isotopic exchange experiments, Howe and co-workers suggested an initial reversible weak adsorption of H<sub>2</sub> resulting in H atoms interacting with Zn sites. These species could react with spin traps and be detected by EPR suggesting radical-like character. The signatures of these radical species were absent in the presence of alkene substrates suggesting either blocking of the sites by alkenes or their involvement in the hydrogenation process rather than or in addition to strongly bound surface (H<sub>(s)</sub>\*) species.

[a] H. Rogers, S. J. Freakley  
Department of Chemistry, University of Bath, Claverton Down, Bath BA2 2AY, UK  
E-mail: s.freakley@bath.ac.uk

[b] T. J. Woodman  
Department of Life Sciences, University of Bath, Claverton Down, Bath BA2 2AY, UK

[c] D. J. Willock, A. Folli  
Cardiff Centre on the Fundamentals of Heterogeneous Catalysis FUNCAT,  
Cardiff Catalysis Institute, School of Chemistry, Cardiff University, Main Building, Park Place, Cardiff CF10 3AT, UK

Supporting information for this article is available on the WWW under <https://doi.org/10.1002/cctc.202401969>

© 2025 The Author(s). ChemCatChem published by Wiley-VCH GmbH. This is an open access article under the terms of the [Creative Commons Attribution License](#), which permits use, distribution and reproduction in any medium, provided the original work is properly cited.

These spin-trapping studies were extended by Carley et al. in 1994 to alkene hydrogenation using Pd/Al<sub>2</sub>O<sub>3</sub> catalysts.<sup>[10]</sup> On exposure of the Pd catalyst to H<sub>2</sub> and either ethene or benzene – alkyl and aromatic free radical intermediates could be detected by spin trapping experiments using *n*-tert-butyl-phenylnitron (PBN) as a spin trap. In the absence of hydrocarbons, the signature of H-PBN<sup>•</sup> free radicals was observed on the Pd catalysts. Supporting desorption and isotopic experiments suggested the H<sup>•</sup> atoms reacting with the spin traps are not strongly chemisorbed hydrogen (H<sub>(s)</sub><sup>•</sup>) but those weakly adsorbed H-adatoms (H<sub>(w)</sub><sup>•</sup>) in equilibrium with H<sub>2(g)</sub>. The observation of ethyl radicals and the absence of H<sup>•</sup> radical signals in the presence of gas phase substrate support a proposed mechanism involving a gas-like overlayer composed of weakly adsorbed ethene reacting and consuming weakly adsorbed H adatoms (H<sub>(w)</sub><sup>•</sup>). This also supported other proposals that strongly adsorbed ethene has low activity in alkene hydrogenation reactions.<sup>[11]</sup> Whilst these studies probed gas phase hydrogenation reactions, in all cases the spin trap molecule is introduced in either toluene or dichloromethane solution after reactant exposure. This suggests that H<sup>•</sup> radicals can be trapped from the catalyst surface in the liquid phase and could also be produced in liquid-phase hydrogenation reactions. Maher and co-workers performed analogous alkene hydrogenation studies to Carley using a liquid phase system by bubbling H<sub>2</sub>-N<sub>2</sub> mixtures and showed the formation of trapped H<sup>•</sup> species by reaction of molecular H<sub>2</sub> with the Pd surface in the liquid phase when a flow of H<sub>2</sub> is introduced.<sup>[12]</sup> The authors concluded that these surface hydrogen ad-atoms must have considerable radical character otherwise spin trapping would not be possible and they are unlikely to be interstitial or covalently bound hydrogen species. The signal of the hydrogen spin-adduct was either considerably diminished or lost completely in the presence of alkenes suggesting the removal of the hydrogen ad-atoms by reaction with the alkene in the liquid phase.

High-loaded Pd/C is frequently used to perform liquid-phase hydrogenations in organic fine synthesis in solvents such as *p*-xylene, THF, and toluene which are thought to be inert. The possible presence of H-ad atoms with significant radical character is often not mechanistically considered and the literature surrounding spin trapping of intermediates in hydrogenation chemistry is scarce since the publications of Carley and Maher, but their presence could have significant implications in H/D scrambling reactions and activation of functional groups. In the studies reported to date, the possible reaction of H<sub>(w)</sub><sup>•</sup> with radical character and the solvent molecules is not considered or conditions more relevant to liquid phase hydrogenations such as elevated temperature and pressure.

Our interest in the mechanisms of (de)hydrogenation reactions on Pd nanoparticles originated from the study of the acceptorless dehydrogenation of 1-phenylethanol to produce molecular H<sub>2</sub>. This reaction was studied using commercial Pd/C catalysts by Nicolau et al. who reported an activation energy of 98 kJ mol<sup>-1</sup> suggesting that C–H cleavage is involved in the rate determining step.<sup>[13]</sup> Additional studies on benzyl alcohols with deuterated benzylic C–H bonds showed a kinetic isotope effect ~1.6; however, the magnitude is lower than typ-

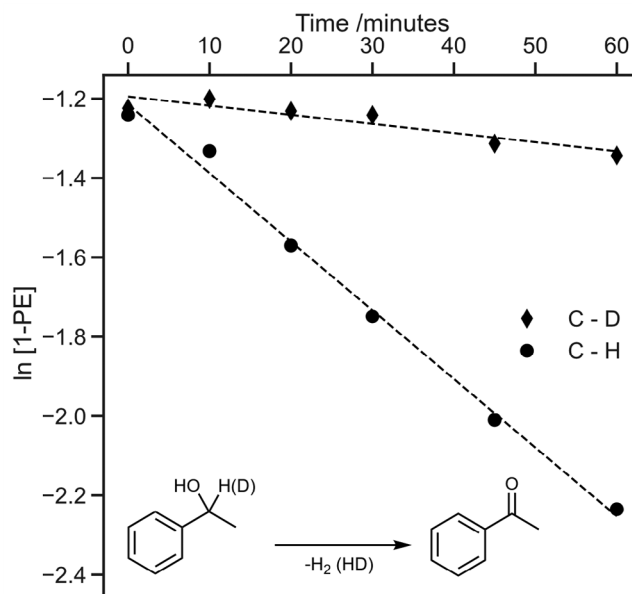


**Figure 1.** Kinetic isotope effect of deuteration of the  $\alpha$ -carbon in 1-phenylethanol acceptorless dehydrogenation. **Conditions:** 120 °C, 1000 rpm, 0.355 M 1-phenylethanol, 20 mg catalyst (1%/Pd/TiO<sub>2</sub>), 10 ml *p*-xylene, flowing Ar.

ically observed for C–H bond cleavage.<sup>[14]</sup> This could indicate second-order effects where the deuterated bond is not directly involved in the rate-determining step, however, the reactions were conducted under a static inert atmosphere meaning ineffective removal of H<sub>2</sub> could also affect the measured rates due to re-hydrogenation of the formed carbonyl. Through a series of catalytic studies using isotopically labelled substrates analysed using <sup>1</sup>H/<sup>2</sup>H Nuclear Magnetic Resonance (NMR) and Electron Paramagnetic Resonance (EPR) spectroscopies with supporting Density Functional Theory (DFT) calculations we probe the presence of these weakly bound H<sub>(w)</sub><sup>•</sup> species under commonly used mild hydrogenation conditions and study the stability of a range of C–H bonds under these conditions.

## 2. Results and Discussion

To conduct our initial studies, we prepared 1-phenylethanol deuterated at the  $\alpha$ -carbon by reducing acetophenone with NaBD<sub>4</sub> followed by acidic workup, mono deuteration at the  $\alpha$ -carbon was confirmed by solvent suppressed <sup>1</sup>H in CDCl<sub>3</sub> and <sup>2</sup>H NMR in C<sub>6</sub>H<sub>6</sub> (Figure S1). Whilst the signals in <sup>2</sup>H NMR are broader than in <sup>1</sup>H NMR, coupling patterns can still be resolved and used to identify the presence and position of isotopic substitution which makes the technique a valuable tool in mechanistic studies. Using a 1% Pd/TiO<sub>2</sub> catalyst which we have previously reported for this reaction, we initially studied acceptorless dehydrogenation of the labelled 1-phenylethanol in *p*-xylene at 120 °C under flowing Ar relative to the unlabelled substrate.<sup>[15]</sup> Figure 1 reveals a large kinetic isotope effect ~7.5, ( $k_H = 0.0170 \text{ min}^{-1}$  and  $k_D = 0.0023 \text{ min}^{-1}$ ) suggesting that the breaking of the  $\alpha$ -carbon-hydrogen bond is likely the rate-determining step to

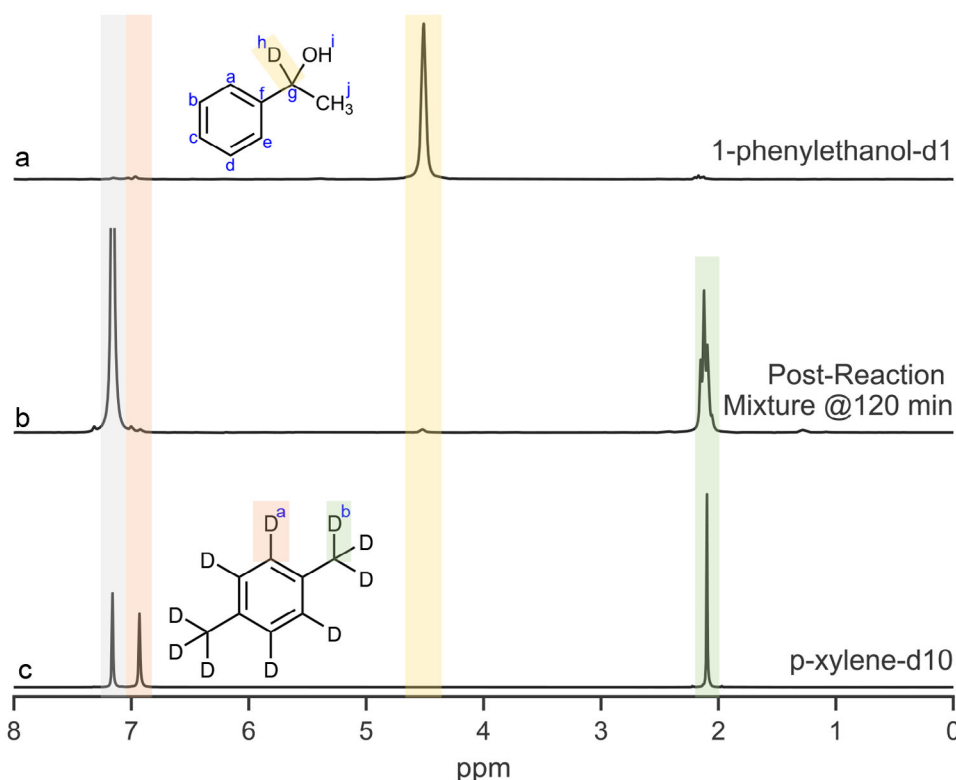


**Figure 2.** (a)  $^2\text{H}$  NMR of mono deuterated 1-phenylethanol starting material, (b) post acceptorless dehydrogenation reaction solution, and (c) p-xylene  $\text{d}^{10}$  reference. Top –  $^2\text{H}$  NMR (77 MHz, no solvent)  $\delta$  4.61 (s, 1D, h). Middle –  $^2\text{H}$  NMR (77 MHz,  $\text{C}_6\text{D}_6$ ),  $\delta$  4.61 (s),  $\delta$  2.19–1.98 (m). Bottom –  $^2\text{D}$  NMR (77 MHz,  $\text{C}_6\text{D}_6$ ),  $\delta$  7.12 ( $\text{C}_6\text{D}_6$  standard) (s),  $\delta$  6.89 (s, 4D),  $\delta$  2.12 (s, 6D, b). **Conditions for reaction in (b):** 120 °C, 1000 rpm, 0.355 M 1-phenylethanol- $\text{d}^{11}$  20 mg catalyst (1%/Pd/TiO<sub>2</sub>), 10 ml p-xylene, flowing Ar.

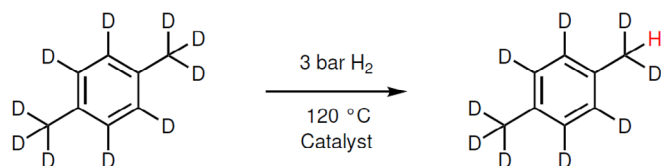
produce H<sub>2</sub> in this system. Generally, values between 2 and 7 (at 298 K) indicate the breaking of a C–H bond and is strongly effected by bond strength, steric effects, solvent effects, and variations in the reaction mechanism depending on the catalyst system.<sup>[16]</sup> The values are in line with studies of acetone production from acceptorless dehydrogenation of IPA when the  $\alpha$ -C–H is deuterated.<sup>[14]</sup>

Figure 2 shows analysis of the reaction mixture after 120 mins by  $^2\text{H}$  NMR. Unexpectedly, in all reactions, a new  $^2\text{H}$  resonance appeared at 2.1–2.2 ppm. The low chemical shift suggests this does not arise from hydrogenation or exchange at the aromatic C–H positions (6.8 ppm) of the substrate when compared to  $\text{C}_6\text{D}_6$  used as an internal reference (7.2 ppm), rather this suggests aliphatic C–D bonds which cannot result from the re-hydrogenation of the formed ketone. A  $^2\text{H}$  NMR of p-xylene- $\text{d}^{10}$  shows a resonance in the same position as the unknown peak consistent with the methyl C–D environment of deuterated p-xylene- $\text{d}^{10}$ . Contaminant  $\text{C}_6\text{D}_6$  resonances (7.2 ppm) was also present in all p-xylene- $\text{d}^{10}$  samples tested. Whilst the p-xylene used as a solvent in the KIE experiments was fully proton form, the position and splitting of the new resonance in the final reaction solutions suggest p-xylene with a single H/D substitution on the methyl group. Throughout our experiments, we did not observe H/D exchange by  $^2\text{H}$ -NMR on aromatic or methyl groups of 1-phenylethanol.

Various methods have been reported to prepare deuterated alkyl aromatics, typically including chlorinated starting materials,

activation of C–H bonds by  $\text{BF}_3/\text{D}_2\text{O}$  or homogeneous catalytic systems such as Ir pincer complexes by C–H insertion.<sup>[17–19]</sup> Approaches using hydrogenation catalysts with high pressures of  $\text{D}_2$  and elevated temperatures often encounter the challenge of avoiding hydrogenation of the aromatic ring or C–C hydrogenolysis. This observation implies that under relatively mild conditions (120 °C, flowing Ar 1 atm) with only the low concentration of HD/ $\text{D}_2$  produced from acceptorless dehydrogenation, the catalyst can activate the methyl C–H bonds of p-xylene under reducing conditions and install a D atom – an observation that will be missed in all liquid phase hydrogenations that use proteo solvents and  $^1\text{H}$  NMR as the H/C–H exchange is not observable.

A wide variety of metal surfaces have been shown to catalyse H/D exchange in C–H bonds since the early studies of Taylor on nickel-kieselguhr catalysts for methane deuteration.<sup>[20,21]</sup> Typically, these reactions are carried in the gas phase at a temperature between 150 and 300 °C, with collected experimental results showing that the reactivity of various alkanes can be understood based on C–H bond dissociation energy (BDE). Studies by Kembel on Pd surfaces report initial C–H activation being the rate-determining step with activation energies for  $\text{CH}_4$  mono-deuteration between 92 and 140  $\text{kJ mol}^{-1}$  and for propane 99  $\text{kJ mol}^{-1}$  which is similar in magnitude to the measured activation energy of 1-phenylethanol acceptorless dehydrogenation, supporting C–H activation as the RDS.<sup>[22]</sup>



Scheme 1. Exchange of methyl deuterium on xylene solvent molecules.

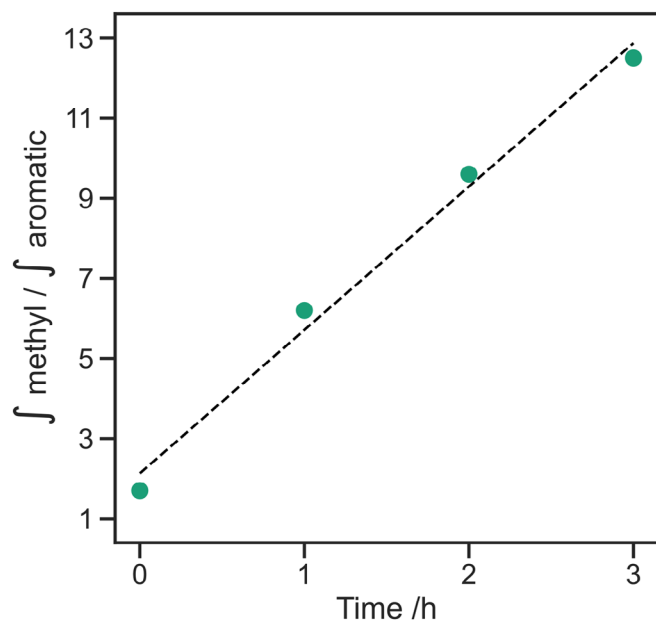


Figure 3. Ratio of aromatic to methyl signals as a function of reaction time determined by  $^1\text{H}$  NMR of the reaction mixture in  $\text{C}_6\text{D}_6$ . Aromatic C-H signal at 6.89 ppm, methyl C-H signal at 2.1 ppm. Conditions: 120 °C, 1000 rpm, 3 bar  $\text{H}_2$ , 20 mg catalyst (1%/Pd/ $\text{TiO}_2$ ), 10 ml p-xylene- $\text{d}^{10}$

We conducted a further set of experiments to identify if the observed C–H(D) activation of the p-xylene solvent during our catalytic reaction is related to 1-phenylethanol acceptorless dehydrogenation. In this set of experiments, we stirred p-xylene- $\text{d}^{10}$  under 3 bar  $\text{H}_2$  at 120 °C with no catalyst, bare  $\text{TiO}_2$  and 1%/Pd/ $\text{TiO}_2$  (Scheme 1) (Figure S2). This revealed that the H/D exchange was only observed when the Pd nanoparticles were present, suggesting that the C–D/H exchange with the gas phase was only possible with concurrent  $\text{H}_2$  activation over the metal surface.

Analysis by  $^1\text{H}$ -NMR spectroscopy of the reaction containing p-xylene- $\text{d}^{10}$  and 1% Pd/ $\text{TiO}_2$  under 3 bar  $\text{H}_2$  pressure at 120 °C initially shows only small residual aromatic and methyl C–H from incomplete deuteration of the solvent as purchased as seen in Figure S3 and Pd free control reactions (Figure S2). Over the course of 3 h the residual aromatic C–H integral (6.95 ppm) remains constant whereas the methyl C–H integral (2.2 ppm) increases linearly over time (Figure 3) indicating increasing H/D exchange of the methyl groups of the solvent over time. This result suggests that in the background of many liquid phase hydrogenation reactions solvent/gas phase exchange at methyl C–H bonds is occurring at the catalyst surface irrespective of substrate conversion.

After showing Pd/ $\text{TiO}_2$  can facilitate this reaction, other nanoparticle catalysts commonly used in hydrogenation (Com-

Table 1. Ratio of integrated methyl and aromatic peaks of  $^1\text{H}$  NMR for p-xylene- $\text{d}^{10}$  following reaction at 120 °C under 3 bar  $\text{H}_2$  for 2 h in the presence of various catalysts.

Catalyst	$\int \text{methyl} / \int \text{aromatic}$
5% Pd/C	112
5% Pt/C	15
2.5% Au/C	2
1% AuPd/ $\text{TiO}_2$	35
1% Au/ $\text{TiO}_2$	2

mercial 5% Pd/C, Synthesised – 5% Pt/C, 2.5% Au/C, 1% AuPd/ $\text{TiO}_2$ , and 1% Au/ $\text{TiO}_2$ ) were investigated for H/D exchange of p-xylene- $\text{d}^{10}$  at 120 °C under 3 bar  $\text{H}_2$ . The relative integral of the aromatic and methyl peaks was used as an indication of H/D exchange, which are summarised in Table 1.

Both Au/C and Au/ $\text{TiO}_2$  showed little to no H/D exchange over the course of the 3 h reaction, and only small amounts of 1,4-dimethylcyclohexane are detected (Figure S4) consistent with Au having a high barrier to  $\text{H}_2$  activation.<sup>[23]</sup> The Pt/C catalyst yielded mainly hydrogenation products, with only a small increase in the integral of the p-xylene methyl group as compared to the aromatic signal. The best catalysts for H/D exchange were 5%Pd/C and 1%AuPd/ $\text{TiO}_2$ ; whilst both spectra show a high methyl/aromatic integral ratio compared to other catalysts suggesting Pd, the most used hydrogenation catalyst, is particularly effective for this H/D exchange of the solvent.

While H/D exchange occurs at the methyl C–H groups preferentially to the aromatic C–H in p-xylene, likely due to the differences in BDEs between the aromatic and benzylic C–H, other solvents were tested to determine if this observation is general across “inert” solvents commonly used in hydrogenation reactions. Initially, toluene- $\text{d}^8$  was tested and showed significant H/D exchange at the benzylic carbon in the presence of the Pd catalyst and 2 bar  $\text{H}_2$  at 100 °C (Figure 4). Analysis of the  $^1\text{H}$  NMR spectra of the residual protons in commercial toluene- $\text{d}^8$  before and after reaction shows a significant increase of C–H at the benzylic position relative to the aromatic C–H signal by ~45x, while the ratio of the integrals between the three aromatic environments remained constant before and after reaction suggesting no H/D exchange on the aromatic ring.

Further experiments using  $\text{D}_2$  and proteo solvents allowed us to probe a variety of solvents, not just those deuterated solvents made widely available for NMR such as p-xylene- $\text{d}^{10}$ . Ethylbenzene was tested to determine selectivity towards benzylic ( $\text{CH}_2$ ) or aliphatic ( $\text{CH}_3$ ) position. The  $^2\text{H}$  NMR (Figure S5a) shows deuterium substitution in only one resonance (3.44 ppm). The splitting pattern observed (doublet of quartets) suggests that the deuterium atom is situated on the benzylic carbon. The 3 methyl protons split the deuterium signal into a quartet with a coupling constant of 1.2 Hz, and the proton on the benzylic carbon splits the signal into a doublet with a larger coupling constant of 2.7 Hz. Further evidence of substitution on the benzylic carbon is shown in the  $^{13}\text{C}$  NMR (Figure S5b). The singlet at 28.94 ppm indicates the benzylic carbon with no deuterium

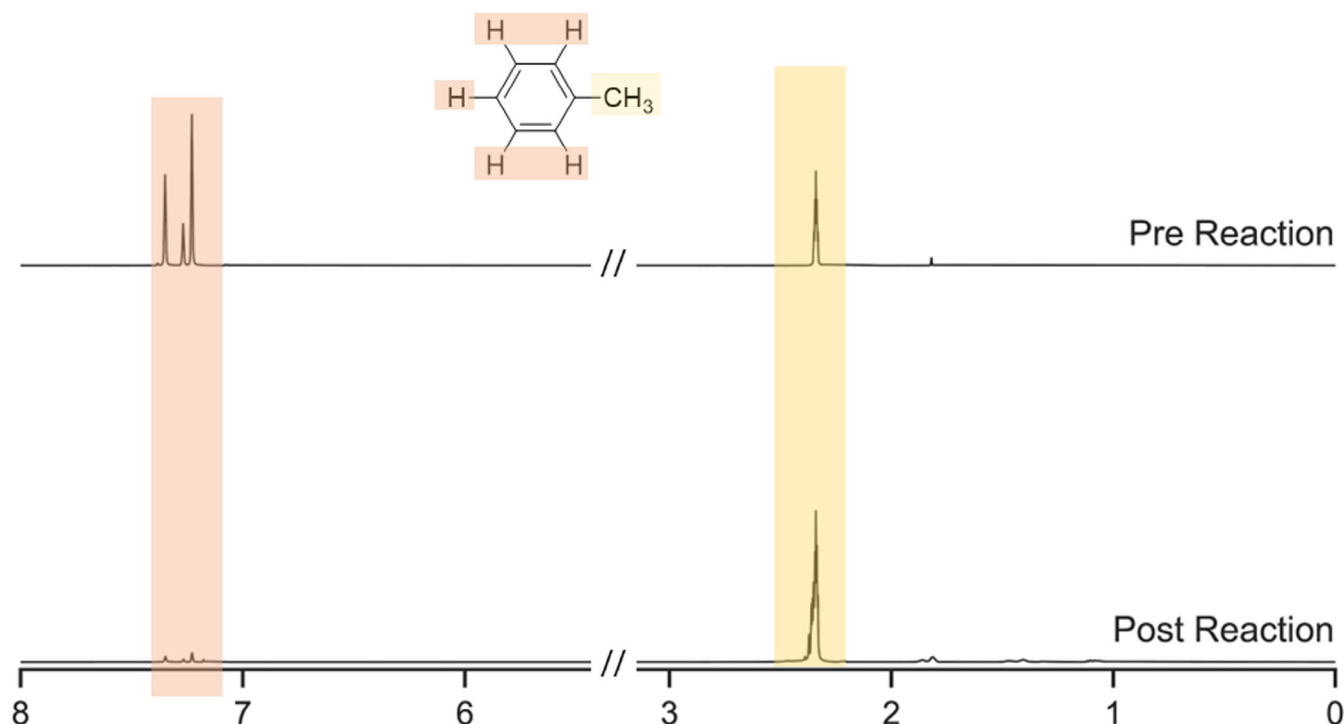


Figure 4-.  $^1\text{H}$  NMR spectra of toluene- $\text{d}^8$  before and after being stirred with a 1% Pd/  $\text{TiO}_2$  catalyst, 3 h, 2 bar  $\text{H}_2$ , 100  $^\circ\text{C}$ .

substitution. The adjacent 1:1:1 triplet at 28.59 ppm is representative of a single deuterium substitution, whilst the low-intensity quintet at 28.24 ppm is indicative of both benzylic protons being substituted for deuterium. Benzene was tested and as expected no exchange was observed before and after reaction (Figure S6a). Cyclohexane, which has a higher BDE (400  $\text{kJ mol}^{-1}$ ) compared to either toluene or xylene methyl groups (313 and 323  $\text{kJ mol}^{-1}$  respectively) and without benzylic carbons also showed no H/D exchange (Figure S6b).

As our results suggest the benzylic position of solvent molecules is particularly susceptible to this background H/D exchange in hydrogenation reactions, radical reaction pathways could be considered as a means of C–H activation via H-abstraction. The production of benzyl and xyl radicals by photolysis or H-abstraction has been well studied in atmospheric chemistry through reaction with OH or Cl radicals. This photochemical gas phase C–H oxidation pathway has shown that H abstraction from benzylic carbon by OH has a low barrier.<sup>[24–26]</sup> It has been shown that weakly bound hydrogen species with a radical-like character can be formed on metal surfaces and are able to react with organic molecules adsorbed to the catalyst surface which could include H-abstraction of activated benzylic positions on solvent molecules. Further reactions were carried out in the presence of *n*-tert-butyl-phenylnitron (PBN) a known spin trap for H-centred radicals. As any hydrogen radicals in our system would be short-lived, a spin trap (PBN) was used to create a persistent PBN-H aminoxyl radical adduct which could be subsequently detected by electron paramagnetic resonance. EPR experiments were carried out with the catalyst, toluene and spin trap (PBN) under 2 bar of  $\text{H}_2$ . As PBN is unstable at elevated temperatures, the reaction time was shortened so any radicals

could be trapped and observed before the spin trap thermally decomposed.

Simulations of the expected EPR spectra for the PBN-H adduct show nine lines should be observed as the nitrogen splits the resonance into a 1:1:1 triplet, in which each peak is further split into a 1:2:1 triplet by adjacent hydrogen. The hyperfine coupling constant of the nitrogen is 1.499 mT, approximately double that of the hydrogen hyperfine coupling constant (0.749 mT). This means some lines overlap to give the seven-line spectra shown (Figure 5a). These values are consistent with literature values for a PBN-H aminoxyl radical adduct in toluene.<sup>[27]</sup> For each catalyst tested in our system an identical seven-line isotropic spectra of varying intensity was observed indicating the presence of H radicals in the system (Figure 5b). The spectra obtained support data collected using NMR. Pt/C, AuPd/ $\text{TiO}_2$ , Pd/C, and Pd/ $\text{TiO}_2$  were all active catalysts for hydrogen/deuterium exchange, evidenced by an increase in the ratio of methyl: aromatic peak integrals. While experimental evidence has been reported to support the presence of weakly absorbed H species on nanoparticle Au surfaces resulting from alcohol dehydrogenation under a  $\text{H}_2$  atmosphere no such species were trapped suggesting that the radicals originate from  $\text{H}_2$  cleavage consistent with the lack of H/D exchange.<sup>[28]</sup> In our studies no PBN adducts of toluene species were detected, which could be due to multiple factors, such as the flux of hydrogen radicals could be significantly higher than the flux of carbon-centred radicals meaning that PBN adducts are statistically unlikely to form and are not observed. Another reason, which is also suggested by Lutterloh et al., is that when the toluene radical intermediate is formed it is adsorbed strongly onto the catalyst surface so cannot react with PBN in the solution.<sup>[29]</sup> A hypothesis supported

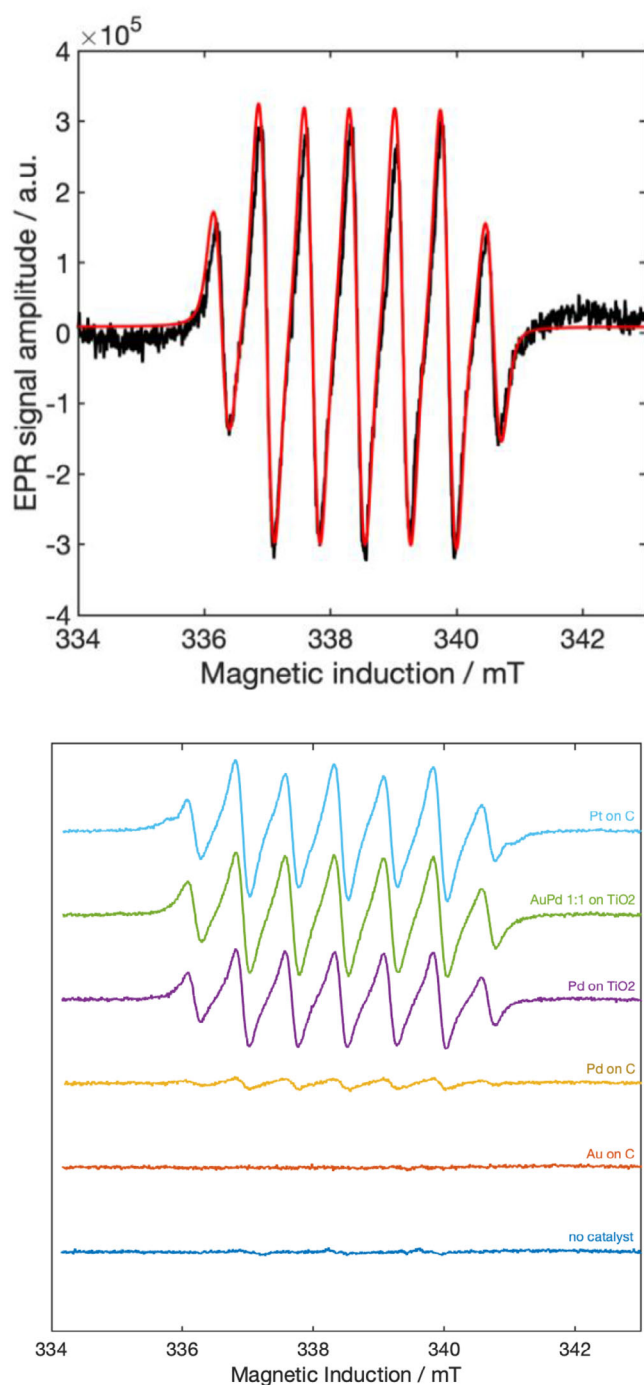


**Figure 5.** (a) Simulation of the PBN-H aminoxyl radical adduct in the fast motion regime (red) compared to experimentally observed signal. (b) X band continuous wave (CW) RT EPR spectra recorded at 100 kHz field modulation frequency, 0.1 mT field modulation amplitude, and 3.17 mW microwave power with 5 spectra averaged per reported spectra.

by the theoretical models of Scaiano who proposed a significant binding energy ( $-116 \text{ kJ mol}^{-1}$ ) of toluene- $\text{CH}_2^*$  to Pd surfaces.<sup>[30]</sup>

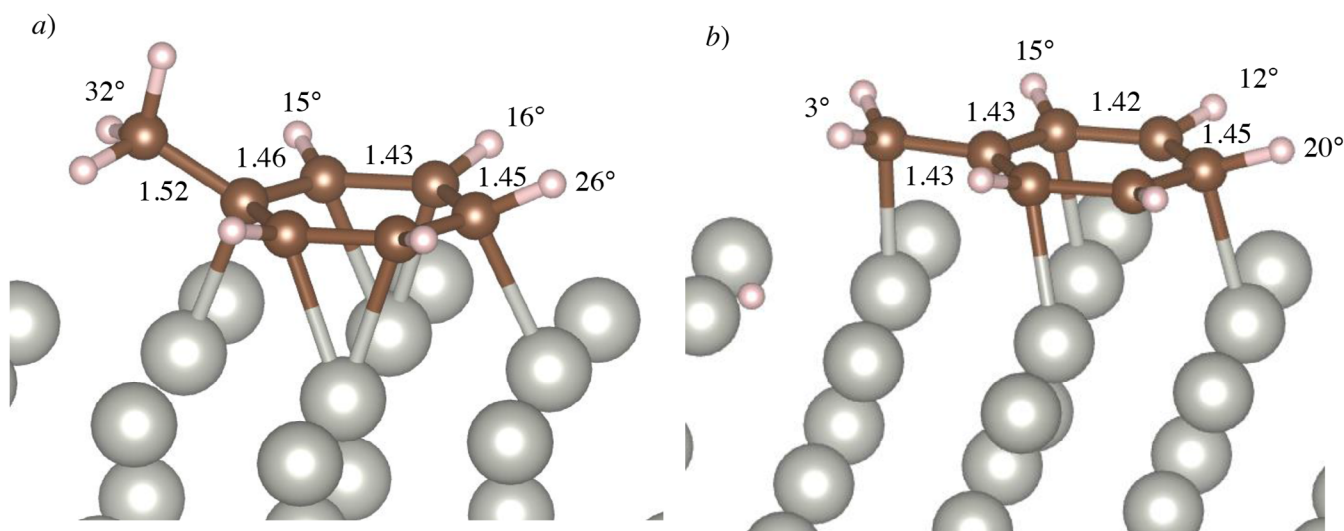
Our own DFT calculations also considered the adsorption of toluene and the radical  $\text{C}_6\text{H}_5\text{CH}_2^*$  to Pd surfaces. Scaiano used the Perdew-Burke-Ernzerhof (PBE) functional without the dispersion corrections included. In our calculations, the adsorp-

tion energies of toluene and the toluene radical with dispersion included (PBE-D3) are even more favourable with  $E_{ads}(g) = -208 \text{ kJ mol}^{-1}$  on the Pd(111) surface with respect to gas phase toluene and with reference to the liquid phase, we obtain  $E_{ads}(l) = -130 \text{ kJ mol}^{-1}$ , which is more relevant to the experiments presented here.

In the adsorbed state the substituents on the toluene aromatic ring move out of plane (Figure 6a). To quantify this effect, we calculate the mean plane of the aromatic carbon atoms and then measure the angle,  $\Theta_{bp}$ , between the bonds to ring substituents and the plane. For toluene on the Pd(111) surface  $\Theta_{bp}$  for the methyl group,  $\Theta_{bp}(\text{C-CH}_3) = 32^\circ$ , is notably larger than for the hydrogen atoms on the ring which averages to  $\Theta_{bp}(\text{C-H}) = 18^\circ$  (Table 2). This is likely due to steric interactions between the methyl group and the surface. Figure 6b shows the optimised structure for the Pd(111) adsorbed radical species,  $\text{C}_6\text{H}_5\text{CH}_2^*$ . In this case, the carbon atom of the methylene radical forms a bond to a surface Pd atom and moves back into the plane of the aromatic ring ( $\Theta_{bp}(\text{C-CH}_2) = 3^\circ$ ) while the movement of the C-H bonds out of the plane of the aromatic ring is similar to that seen in toluene (av.  $\Theta_{bp}(\text{C-H}) = 15^\circ$ , Table 2). We also note that the C-C bond between the methylene group and the aromatic ring is significantly shorter than seen for the methyl group of toluene, suggesting a degree of conjugation between the  $\text{CH}_2$  substituent and the ring in the radical.

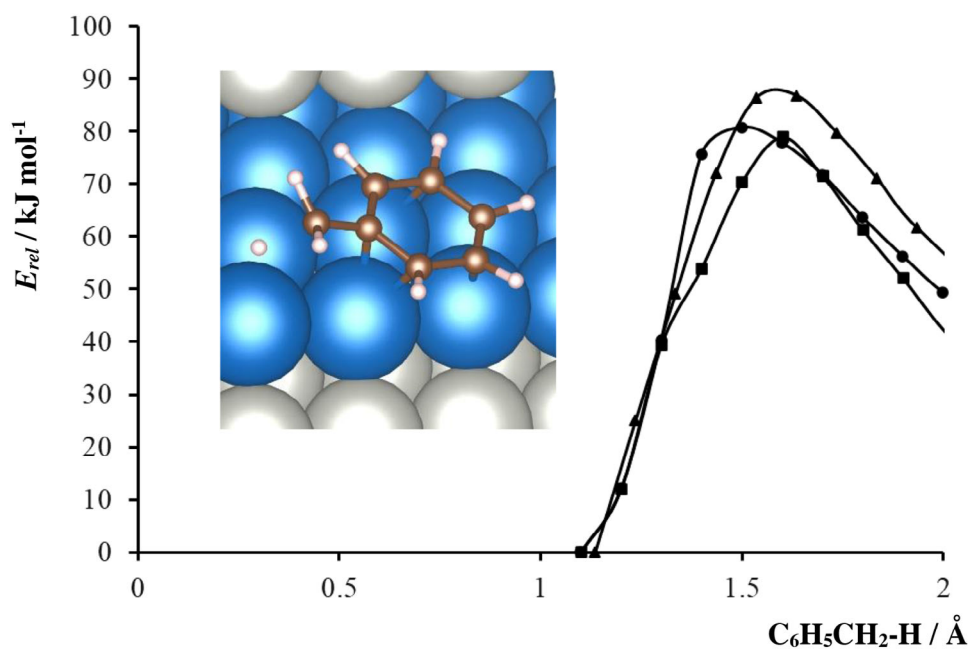
For the stepped Pd(211) surface, we also consider adsorption of toluene with the methyl group orientated towards the step edge (step, Figure S8a) and with the aromatic ring to methyl group bond parallel to the step edge (terrace, Figure S8c). The adsorption energy for toluene in the step site shows a small enhancement compared to the planar Pd(111) surface by  $7 \text{ kJ mol}^{-1}$  while adsorption on the terrace site has a calculated energy of some  $3 \text{ kJ mol}^{-1}$  less stable. These small energy differences suggest that toluene adsorption through the aromatic ring is largely site independent and we would expect toluene to adsorb to most of the available surface sites on a typical Pd nanoparticle. At the step site, when a  $\text{C}_6\text{H}_5\text{CH}_2^*$  radical is formed the methylene carbon is co-ordinated to a Pd atom at the top edge of the step (Figure S8b) and so the bond angle for the methylene group with respect to the aromatic ring, remains similar to that for the toluene molecule in the same adsorption site ( $\Theta_{bp}(\text{C-CH}_2) = 22^\circ$  cf  $\Theta_{bp}(\text{C-CH}_3) = 25^\circ$ ). On the terrace site (Figure S8d) the geometry of the radical adsorbate is quite similar to that seen for Pd(111) with the methylene carbon atom closer to the plane of the aromatic ring.

Figure 7 shows the reaction barriers calculated for each adsorption site. The step edge is found to have the highest barrier to  $\text{C}_6\text{H}_5\text{CH}_2\text{-H}$  cleavage of any of the systems studied at  $87 \text{ kJ mol}^{-1}$  compared to around  $80 \text{ kJ mol}^{-1}$  for the Pd(211) terrace and Pd(111) surfaces. These barriers are notably lower than discussed earlier for the dehydrogenation of 1-phenyl ethanol suggesting that if hydrogen transfer involving the aromatic alcohol is taking place, then the exchange of H atoms with toluene solvent molecules should also be expected.



**Figure 6.** Calculated structures at the PBE-D3 level for (a) toluene and (b) a  $C_6H_5CH_2^\bullet$  radical, adsorbed to the Pd(111) surface. C-C bond distances are given in Å, angles between bonds and mean aromatic plane,  $\Theta_{bp}$ , are written at the end of bonds. Atom colours: Pd : grey, C : Brown, H: white.

Table 2. Calculated energies and geometric factors for toluene and toluene- $CH_2^\bullet$ adsorption to Pd(111) and Pd(211).							
Surface	Site	Adsorbate	$E_{ads}(g) / \text{kJ mol}^{-1}$	$E_{ads}(l) / \text{kJ mol}^{-1}$	$E_{act} / \text{kJ mol}^{-1}$	$\Theta_{bp}(C-CH_3) / ^\circ$	$\Theta_{bp}(C-H) / ^\circ$
Pd (111)		$C_6H_5CH_3$	-208	-130	81	32	18
		$C_6H_5CH_2^\bullet$	-235	-157	–	3	15
Pd (211)	step	$C_6H_5CH_3$	-214	-137	87	25	18
	terrace	$C_6H_5CH_3$	-204	-127	79	6	17
	step	$C_6H_5CH_2^\bullet$	-198	-121	–	22	19
	terrace	$C_6H_5CH_2^\bullet$	-227	-150	–		



**Figure 7.** Calculated barriers for  $C_6H_5CH_2-H$  bond cleavage over Pd(111) (circles), Pd(211) step (triangles) and Pd(211) terrace (squares). Energy is taken relative to the adsorbed toluene state in each case. Inset graphic shows the calculated transition state for Pd(211) terrace. Atom colours: Pd : grey, with terrace atoms blue, C : Brown, H: white.

### 3. Conclusions

Using isotopic labelling and  $^2\text{H}$  NMR we show that under commonly used hydrogenation conditions (120 °C, 3 bar  $\text{H}_2$ ) in the presence of Pd/C catalysts C-H/D exchange occurs in solvent molecules (toluene, xylene), particularly at the benzylic positions. This observation is only possible when using combinations of  $\text{H}_2/\text{D}_2$  with proteo/deuterated solvents and both  $^1\text{H}$  and  $^2\text{H}$  NMR. This process is likely occurring undetected in all liquid-phase hydrogen processes that utilize common proteo solvents which employ only  $^1\text{H}$ -NMR for analysis. In addition, our DFT studies suggest that carbon-centered radicals derived from solvent activation can bind strongly to Pd surfaces and have reasonable activation barriers to C-H activation compared to many target substrates. This suggests that the presence of strongly bound solvent molecules with radical character should be considered in models of catalytic reactions at surfaces. We show that under these conditions in the presence of catalysts that are known for facile activation of  $\text{H}_2$  we can trap H-radical adducts using spin-trapping EPR and these species could play mechanistic roles in numerous catalytic processes.

### 4. Experimental Methods

Chemicals were supplied by Sigma Aldrich and used without further purification unless otherwise stated.

#### 4.1. Catalyst Synthesis – 1% Pd/TiO<sub>2</sub>

Using a 500 mL round-bottomed flask Ar was bubbled through 400 mL of de-ionised water whilst vigorously stirring for 30 minutes. An acidic (0.5 M HCl) aqueous solution of  $\text{PdCl}_2(\text{aq})$  (1.7 mL, 6 mg  $\text{mL}^{-1}$  Pd) was added using a syringe followed by an aqueous solution of polyvinyl alcohol (Mw 9000 – 10000, 1.2 mL, 1% wt.) so that the metal:PVA mass ratio was 1:1.2. After 2–3 minutes a freshly prepared aqueous solution of  $\text{NaBH}_4$  (4.7 mL, 0.1 M) was added such that the metal: $\text{NaBH}_4$  molar ratio was 1:5. After stirring for a further 30 minutes  $\text{TiO}_2$  (990 mg, Degussa p25) was added, followed by concentrated  $\text{H}_2\text{SO}_4$  (6 drops). The suspension was stirred for 1 h before being filtered and washed with water. The catalyst was then dried in air at 110 °C for 16 h. **1% Au / TiO<sub>2</sub> and 1% AuPd/TiO<sub>2</sub>** were prepared by a similar method using  $\text{HAuCl}_4$  as the gold precursor. **5% Pt/C** was prepared by a similar method using  $\text{H}_2\text{PtCl}_6 \cdot 2\text{H}_2\text{O}$  and Norit GSX as the carbon support. **2.5% Au/C** was prepared by a similar method using  $\text{HAuCl}_4$  as the gold precursor and Norit ROX – as the carbon support. Commercial 5% Pd/C was obtained from Sigma Aldrich.

#### 4.2. Catalyst Testing – Acceptorless Dehydrogenation in an Open System

A solution of 1-phenylethanol in p-xylene (10 mL, 0.4 M) was added to a 2-neck round bottomed flask equipped with a reflux condenser. The system was purged with Ar for 15 minutes, before

being heated to 120 °C and purged for a further 15 minutes. Catalyst (20 mg unless otherwise stated) was added to the flask to give a nominal Pd mol% of 0.05 based on a 1% theoretical metal loading. The reaction was stirred at 1000 rpm under flowing Ar for the duration of the reaction (typically 2 h). Aliquots removed at 30-minute intervals were centrifuged in 2.5 mL sample tubes at 10,000 rpm for analysis using gas chromatography.

#### 4.3. Solvent H/D Exchange

Catalyst (0.05 mg active metal) and solvent (5 mL) were added to a 50 mL glass reactor (Radleys) and connected to a gas supply manifold. The flask was charged with  $\text{H}_2$  (2 bar) and stirred at 120 °C for 3 hours. Samples were filtered using a PTFE syringe filter for analysis by NMR.

#### 4.4. 1-Phenylethanol-d<sup>1</sup> Synthesis

Acetophenone (2 mL) was added dropwise to a solution of  $\text{NaBD}_4$  (0.29 g) in EtOH (6 mL) at 30 °C. This mixture was stirred at 30 °C for 15 minutes before being removed from the heat and quenched with HCl (1 M, 6 mL). The mixture was then heated to 75 °C to allow the EtOH to evaporate and the product to oil out. After cooling, the product was extracted with  $\text{Et}_2\text{O}$  and washed with DI water, and the organic layer was then dried over  $\text{MgSO}_4$  and concentrated in vacuo to give 1-phenylethanol-d<sup>1</sup> (1.7 g, 85% yield). Proton and deuterium NMR confirmed the identity of the product.

#### 4.5. Product Analysis

An Agilent 6890 N GC fitted with a flame ionisation detector was used to analyse reaction mixture samples from the dehydrogenation of 1-phenylethanol and the hydrogenation of acetophenone. An HP-5 (5% phenyl methyl siloxane, capillary (30.0 m  $\times$  320  $\mu\text{m}$   $\times$  0.25  $\mu\text{m}$ )) column was used with  $\text{N}_2$  as a carrier gas. Samples were prepared for analysis by adding 0.5 mL of external standard (biphenyl, 0.2 M) to a 0.5 mL aliquot of reaction mixture. All NMR experiments were performed on a Bruker Avance III spectrometer operating at 500 MHz for  $^1\text{H}$ . Samples of reaction mixture were prepared by filtering through a PTFE syringe filter.  $^2\text{H}$  NMR samples were analysed without further dilution. To a 400  $\mu\text{L}$  sample, 20  $\mu\text{L}$  of a reference compound ( $\text{CDCl}_3$ ,  $\text{C}_6\text{D}_6$ , or MeOD was added).  $^1\text{H}$  NMR and  $^{13}\text{C}$  NMR samples were diluted prior to analysis. To 100  $\mu\text{L}$  of reaction mixture, 400  $\mu\text{L}$  of deuterated solvent ( $\text{CDCl}_3$ ,  $\text{C}_6\text{D}_6$ , or MeOD) was added. NMR spectra were processed using MNova software.

#### 4.6. EPR

Samples were prepared by stirring catalyst (0.05 mg active metal), PBN spin trap (5 mg), and toluene-d<sup>8</sup> (10 mL) under an atmosphere of  $\text{H}_2$  (2 bar) for 10 minutes at 120 °C. Samples were

filtered using a PTFE syringe filter before being loaded into a capillary tube for analysis. EPR experiments were carried out using a Bruker EMX (X-band) spectrometer. Xband continuous wave spectra were recorded at room temperature, with 100 kHz field modulation frequency, 0.1 mT field modulation amplitude, and 3.17 mW microwave power. For each sample the result was taken as the average of 5 spectra. EPR simulations were carried out in the fast motion regime by computing the Breit-Rabi formalism, i.e., the analytical diagonalization of the spin Hamiltonian for a  $S = 1/2$  electron spin system. The following parameters were used:  $g_{\text{iso}} = 2.0056$ ,  $a_{\text{iso}}(14 \text{ N}) = 1.44 \text{ mT}$ ,  $a_{\text{iso}}(^1\text{H}_\beta) = 0.72 \text{ mT}$  (x2).

#### 4.7. DFT

Calculations were carried out using the VASP periodic DFT code with the PBE functional and Grimme D3 dispersion corrections (PBE-D3).<sup>[31–33]</sup> The core states of all atoms were represented using the projector augmented-wave (PAW) approach and a 500 eV plane wave cut-off was used throughout.<sup>[34,35]</sup> The python based Atomic Simulation Environment (ASE) was used for management of calculation geometries.<sup>[36,37]</sup> The fcc bulk unit cell of Pd was first optimised using  $7 \times 7 \times 7$   $k$ -point sampling to give a cubic lattice parameter,  $a = 3.906 \text{ \AA}$ , in excellent agreement with the experimentally determined value ( $a = 3.890 \text{ \AA}$ ).<sup>[38]</sup> The optimised fcc cell was converted to a rhombohedral primitive cell and a  $p4 \times 4$  Pd(111) slab model was created with surface cell vectors  $u = v = 11.191 \text{ \AA}$  and a simulation cell vector perpendicular to the surface of  $29.137 \text{ \AA}$  (Figure S7a). The Pd(111) slab model contained 80 Pd atoms, i.e., 5 layers in the direction perpendicular to the surface so the chosen cell vector corresponds to a vacuum gap of  $20.1 \text{ \AA}$ . To represent a stepped surface, a slab model for Pd(211) was created in the same way with surface cell vectors  $u = 11.037 \text{ \AA}$  and  $v = 13.517 \text{ \AA}$  and a simulation cell vector perpendicular to the surface of  $47.790 \text{ \AA}$  in the direction perpendicular to the surface. This Pd(211) slab model contains 128 atoms, with at least 5 atom thickness at all points on the surface and a vacuum gap of  $35.8 \text{ \AA}$  (Figure S7b). Figure S6c gives a top view of the Pd(211) surface showing that this Miller index choice gives a stepped surface with Pd(111) terrace and Pd(100) step features.

The adsorption energy relative to gas phase toluene,  $E_{\text{ads}}(g)$ , for a structure is calculated using:

$$E_{\text{ads}}(g) = E_{\text{struct}} - E_{\text{slab}} - E_{\text{tol}}(g) \quad (1)$$

where  $E_{\text{struct}}$  is the calculated energy for the optimised adsorbate structure,  $E_{\text{slab}}$  is the calculated energy of the slab model of the clean surface obtained using the same program settings.  $E_{\text{tol}}(g)$  is the reference energy for gas phase toluene obtained from the optimisation of a single toluene molecule in the unit cell used for the Pd(111) surface slab model. This is the usual approach used in the literature and so  $E_{\text{ads}}(g)$  is used for comparison with earlier work. Since the experimental work presented here is carried out in the liquid phase we have also attempted to estimate the adsorption energy relative to liquid phase toluene,  $E_{\text{ads}}(l)$ . In this case, the reference energy is taken from a calculation of toluene

in the condensed phase starting from the  $P2_1/c$  crystal structure reported by Anderson et al.<sup>[39]</sup> This structure was obtained at 165 K with a quoted density of  $1.054 \text{ g cm}^{-3}$ . To obtain an approximation to the liquid phase we expanded the cell to give a density of  $0.87 \text{ g cm}^{-3}$  and then optimised atomic coordinates. This gives an estimate for the interaction energy per molecule in the liquid phase as

$$E_{\text{tol}}(l) = -156 \text{ kJ mol}^{-1} \text{ and so } E_{\text{ads}}(l) \text{ can be obtained using:}$$

$$E_{\text{ads}}(l) = E_{\text{ads}}(g) - \frac{1}{2}E_{\text{tol}}(l) \quad (2)$$

This accounts for the additional energy required for the molecule to move from the liquid state to the surface losing approximately half of the interactions with other molecules in the liquid phase. Note that both definitions imply that negative  $E_{\text{ads}}$  values correspond to favourable adsorption energies.

Transition state searches were carried out using the ASE constrained bond facility. Starting from the optimised structure for toluene on each surface the methyl H atom closest to the surface was selected and the C–H bond extended by  $0.1 \text{ \AA}$ . The structure was then re-optimized with the selected C–H bond constrained to maintain the same length. From the end point of this re-optimisation the same bond was again extended by  $0.1 \text{ \AA}$  before a further optimisation. This process of bond elongation and optimisation was continued until the C.H distance was around  $2 \text{ \AA}$  and a barrier could be seen in the energy profile. The point nearest the top of the barrier was then selected and a frequency calculation carried out to confirm a single negative mode at the transition state. The mode was also animated to confirm that it corresponded to C–H bond cleavage. In frequency calculations the Pd atoms were not included in the numerical evaluation of the Hessian based on the significant mass difference between Pd and C/H. This also reduced the computer time required for frequency calculations.

#### Acknowledgements

The authors have nothing to report.

#### Conflict of Interests

The authors declare no conflict of interest.

#### Data Availability Statement

The data that support the findings of this study are available from the corresponding author upon reasonable request.

**Keywords:** C-H Activation · Hydrogenation · Palladium · Radical

- [1] L. Zhang, M. Zhou, A. Wang, T. Zhang, *Chem. Rev.* **2020**, *120*, 683–733.  
[2] M. A. Stoffels, F. J. R. Klauck, T. Hamadi, F. Glorius, J. Leker, *Adv. Synth. Catal.* **2020**, *362*, 1258–1274.

- [3] X. Zhao, Y. Chang, W. J. Chen, Q. Wu, X. Pan, K. Chen, B. Weng, *ACS Omega* **2022**, *7*, 17–31.
- [4] W. Dong, G. Kresse, J. Hafner, *J. Mol. Catal. A: Chem.* **1997**, *119*, 69–76.
- [5] B. Mattson, W. Foster, J. Greimann, T. Hoette, N. Le, A. Mirich, S. Wankum, A. Cabri, C. Reichenbacher, E. Schwanke, *J. Chem. Educ.* **2013**, *90*, 613–619.
- [6] J. S. Adams, M. L. Kromer, J. Rodríguez-López, D. W. Flaherty, *J. Am. Chem. Soc.* **2021**, *143*, 7940–7957.
- [7] N. M. Wilson, P. Priyadarshini, S. Kunz, D. W. Flaherty, *J. Catal.* **2018**, *357*, 163–175.
- [8] Z. Zhao, R. Bababrik, W. Xue, Y. Li, N. M. Briggs, D.-T. Nguyen, U. Nguyen, S. P. Crossley, S. Wang, B. Wang, D. E. Resasco, *Nat. Catal.* **2019**, *2*, 431–436.
- [9] T. Matsuzaki, T. Uda, A. Kazusaka, G. W. Keulks, R. F. Howe, *J. Am. Chem. Soc.* **1980**, *102*, 7511–7513.
- [10] A. F. Carley, H. A. Edwards, B. Mile, M. W. Roberts, C. C. Rowlands, F. E. Hancock, S. D. Jackson, *J. Chem. Soc., Faraday Trans.* **1994**, *90*, 3341–3346.
- [11] S. J. Thomson, G. Webb, *J. Chem. Soc., Chem. Commun.* **1976**, 526–527.
- [12] A. Burt, M. Emery, J. Maher, B. Mile, *Magn. Reson. Chem.* **2001**, *39*, 85–88.
- [13] G. Nicolau, G. Tarantino, C. Hammond, *ChemSusChem* **2019**, *12*, 4953–4961.
- [14] K. Kon, W. Onodera, T. Toyao, K.-i. Shimizu, *Catal. Sci. Technol.* **2016**, *6*, 5864–5870.
- [15] H. Rogers, I. T. Daniel, S. J. Freakley, *Catal. Commun.* **2022**, *162*, 106377.
- [16] M. Gómez-Gallego, M. A. Sierra, *Chem. Rev.* **2011**, *111*, 4857–4963.
- [17] J. W. Larsen, L. W. Chang, *J. Org. Chem.* **1978**, *43*, 3602–3602.
- [18] J. L. Rhinehart, K. A. Manbeck, S. K. Buzak, G. M. Lippa, W. W. Brennessel, K. I. Goldberg, W. D. Jones, *Organometallics* **2012**, *31*, 1943–1952.
- [19] J. D. Smith, G. Durrant, D. H. Ess, B. S. Gelfand, W. E. Piers, *Chem. Sci.* **2020**, *11*, 10705–10717.
- [20] A. Sattler, *ACS Catal.* **2018**, *8*, 2296–2312.
- [21] K. Morikawa, W. S. Benedict, H. S. Taylor, *J. Am. Chem. Soc.* **1936**, *58*, 1445–1449.
- [22] C. Kemball, R. G. W. Norrish, *Proc. R. Soc. London, Ser. A* **1951**, *207*, 539–554.
- [23] B. Hammer, J. K. Norskov, *Nature* **1995**, *376*, 238–240.
- [24] V. H. Uc, J. R. Alvarez-Idaboy, A. Galano, I. García-Cruz, A. Vivier-Bunge, *J. Phys. Chem. A* **2006**, *110*, 10155–10162.
- [25] S.-X. Hu, J.-G. Yu, S.-M. Li, E. Y. Zeng, *Computational and Theoretical Chemistry* **2011**, *977*, 13–21.
- [26] S. Pan, L. Wang, *J. Phys. Chem. A* **2014**, *118*, 10778–10787.
- [27] G. R. Buettner, *Free Radic Biol Med* **1987**, *3*, 259–303.
- [28] M. Conte, H. Miyamura, S. Kobayashi, V. Chechik, *J. Am. Chem. Soc.* **2009**, *131*, 7189–7196.
- [29] C. Lutterloh, J. Biener, A. Schenk, J. Küppers, *Surf. Sci.* **1995**, *331–333*, 261–266.
- [30] T. A. Gawargy, P. Costa, A. E. Lanterna, J. C. Scaiano, *Org. Biomol. Chem.* **2020**, *18*, 6047–6052.
- [31] G. Kresse, J. Hafner, *Phys. Rev. B* **1993**, *47*, 558–561.
- [32] G. Kresse, J. Furthmüller, *Phys. Rev. B* **1996**, *54*, 11169–11186.
- [33] J. P. Perdew, K. Burke, M. Ernzerhof, *Phys. Rev. Lett.* **1996**, *77*, 3865–3868.
- [34] S. Grimme, J. Antony, S. Ehrlich, H. Krieg, *J. Chem. Phys.* **2010**, *132*, 154104.
- [35] G. Kresse, D. Joubert, *Phys. Rev. B* **1999**, *59*, 1758–1775.
- [36] V. Blum, R. Gehrke, F. Hanke, P. Havu, V. Havu, X. Ren, K. Reuter, M. Scheffler, *Comput. Phys. Commun.* **2009**, *180*, 2175–2196.
- [37] A. Hjorth Larsen, J. Jørgen Mortensen, J. Blomqvist, I. E. Castelli, R. Christensen, M. Dułak, J. Friis, M. N. Groves, B. Hammer, C. Hargus, E. D. Hermes, P. C. Jennings, P. Bjerre Jensen, J. Kermode, J. R. Kitchin, E. Leonhard Kolsbjerg, J. Kubal, K. Kaasbjerg, S. Lysgaard, J. Bergmann Maronsson, T. Maxson, T. Olsen, L. Pastewka, A. Peterson, C. Rostgaard, J. Schiøtz, O. Schütt, M. Strange, K. S. Thygesen, T. Vegge, L. Vilhelmsen, M. Walter, Z. Zeng, K. W. Jacobsen, *J. Phys.: Condens. Matter* **2017**, *29*, 273002.
- [38] J. W. Arblaster, *Platinum Met. Rev.* **2012**, *56*, 181–189.
- [39] M. Anderson, L. Bosio, J. Bruneaux-Pouille, R. Fourme, *J. Chim. Phys.* **1977**, *74*, 68–73.

---

Manuscript received: November 28, 2024  
Revised manuscript received: February 10, 2025  
Accepted manuscript online: February 14, 2025  
Version of record online: April 28, 2025